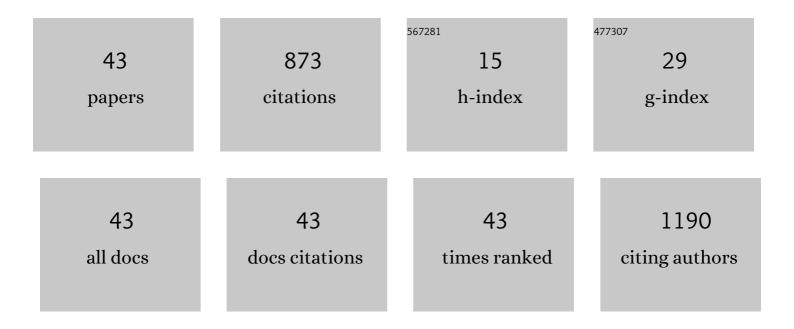


List of Publications by Year in descending order

Source: https://exaly.com/author-pdf/8852103/publications.pdf Version: 2024-02-01



#	Article	IF	CITATIONS
1	Global Sensitivity Analysis of the MEMLS Model for Retrieving Snow Water Equivalent. IEEE Transactions on Geoscience and Remote Sensing, 2022, 60, 1-15.	6.3	4
2	Seasonal snow cover classification based on SAR imagery and topographic data. Remote Sensing Letters, 2022, 13, 269-278.	1.4	3
3	Daily snow water equivalent product with SMMR, SSM/I and SSMIS from 1980 to 2020 over China. Big Earth Data, 2022, 6, 420-434.	4.4	12
4	Wet snow detection using dual-polarized Sentinel-1 SAR time series data considering different land categories. Geocarto International, 2022, 37, 10907-10924.	3.5	4
5	Spatio-temporal analysis of the melt onset dates over Arctic sea ice from 1979 to 2017. Acta Oceanologica Sinica, 2022, 41, 146-156.	1.0	0
6	Uncertainty Characterization of Groundâ€Based, Satellite, and Reanalysis Snow Depth Products Using Extended Triple Collocation. Water Resources Research, 2022, 58, .	4.2	6
7	Comparison of Different Intercalibration Methods of Brightness Temperatures From FY-3D and AMSR2. IEEE Transactions on Geoscience and Remote Sensing, 2022, 60, 1-17.	6.3	4
8	An automatic method for clean glacier and nonseasonal snow area change estimation in High Mountain Asia from 1990 to 2018. Remote Sensing of Environment, 2021, 258, 112376.	11.0	19
9	A Micro-UAV-Radar System for Vegetation Height Inversion: a Feasibility Study. , 2021, , .		0
10	A Method for Mapping Snowmelt Extent with Multitemporal Radar Data. , 2021, , .		0
11	A New Geostationary Satellite-Based Snow Cover Recognition Method for FY-4A AGRI. IEEE Journal of Selected Topics in Applied Earth Observations and Remote Sensing, 2021, 14, 11372-11385.	4.9	5
12	Comparison of HY-2B Passive Brightness Temperatures with SSMI/S, GMI, AMSR2 and MWRI in Land Surface. IOP Conference Series: Earth and Environmental Science, 2020, 502, 012007.	0.3	4
13	Spatial and Temporal Variations of Arctic Sea Ice From 2002 to 2017. Earth and Space Science, 2020, 7, e2020EA001278.	2.6	8
14	An Assessment and Error Analysis of MOD10A1 Snow Product Using Landsat and Ground Observations Over China During 2000–2016. IEEE Journal of Selected Topics in Applied Earth Observations and Remote Sensing, 2020, 13, 1467-1478.	4.9	10
15	Consistent Comparison of Remotely Sensed Sea Ice Concentration Products with ERA-Interim Reanalysis Data in Polar Regions. Remote Sensing, 2020, 12, 2880.	4.0	1
16	Characterizing the surge behavior of Alakesayi Glacier in the West Kunlun Shan, Northwestern Tibetan Plateau, from remote-sensing data between 2013 and 2018. Journal of Glaciology, 2019, 65, 168-172.	2.2	12
17	Improved Maximum Likelihood Estimation for Optimal Phase History Retrieval of Distributed Scatterers in InSAR Stacks. IEEE Access, 2019, 7, 186319-186327.	4.2	5
18	Inter-Sensor Calibration between HY-2B and AMSR2 Passive Microwave Data in Land Surface and First Result for Snow Water Equivalent Retrieval. Sensors, 2019, 19, 5023.	3.8	7

Lizhe

#	Article	IF	CITATIONS
19	A Ground Surface Deformation Monitoring InSAR Method Using Improved Distributed Scatterers Phase Estimation. IEEE Journal of Selected Topics in Applied Earth Observations and Remote Sensing, 2019, 12, 4543-4553.	4.9	17
20	Parameter Optimization of a Discrete Scattering Model by Integration of Global Sensitivity Analysis Using SMAP Active and Passive Observations. IEEE Transactions on Geoscience and Remote Sensing, 2019, 57, 1084-1099.	6.3	22
21	Soil Moisture Retrieval From SMAP: A Validation and Error Analysis Study Using Ground-Based Observations Over the Little Washita Watershed. IEEE Transactions on Geoscience and Remote Sensing, 2018, 56, 1394-1408.	6.3	52
22	A Preliminary Evaluation of the GaoFen-3 SAR Radiation Characteristics in Land Surface and Compared With Radarsat-2 and Sentinel-1A. IEEE Geoscience and Remote Sensing Letters, 2018, 15, 1040-1044.	3.1	13
23	Extraction of Glacial Lake Outlines in Tibet Plateau Using Landsat 8 Imagery and Google Earth Engine. IEEE Journal of Selected Topics in Applied Earth Observations and Remote Sensing, 2017, 10, 4002-4009.	4.9	80
24	Estimation of supraglacial debris thickness using a novel target decomposition on Lâ€band polarimetric SAR images in the Tianshan Mountains. Journal of Geophysical Research F: Earth Surface, 2017, 122, 925-940.	2.8	11
25	Modelling temporal variations in microwave backscattering from reed marshes. International Journal of Remote Sensing, 2017, 38, 6930-6944.	2.9	3
26	Quantification of Temporal Decorrelation in X-, C-, and L-Band Interferometry for the Permafrost Region of the Qinghai–Tibet Plateau. IEEE Geoscience and Remote Sensing Letters, 2017, 14, 2285-2289.	3.1	12
27	Use of Intensity and Coherence of <i>X</i> -Band SAR Data to Map Thermokarst Lakes on the Northern Tibetan Plateau. IEEE Journal of Selected Topics in Applied Earth Observations and Remote Sensing, 2016, 9, 3164-3176.	4.9	7
28	The backscattering characteristics of wetland vegetation and water-level changes detection using multi-mode SAR: A case study. International Journal of Applied Earth Observation and Geoinformation, 2016, 45, 1-13.	2.8	39
29	Permafrost environment monitoring on the Qinghai-Tibet Plateau using time series ASAR images. International Journal of Digital Earth, 2015, 8, 840-860.	3.9	22
30	A level set method for segmentation of high-resolution polarimetric SAR images using a heterogeneous clutter model. Remote Sensing Letters, 2015, 6, 548-557.	1.4	3
31	Evaluation of remotely sensed and reanalysis soil moisture products over the Tibetan Plateau using in-situ observations. Remote Sensing of Environment, 2015, 163, 91-110.	11.0	287
32	A method for monitoring hydrological conditions beneath herbaceous wetlands using multi-temporal ALOS PALSAR coherence data. Remote Sensing Letters, 2015, 6, 618-627.	1.4	15
33	Method for Soil Moisture and Surface Temperature Estimation in the Tibetan Plateau Using Spaceborne Radiometer Observations. IEEE Geoscience and Remote Sensing Letters, 2015, 12, 97-101.	3.1	52
34	Recognition of supraglacial debris in the Tianshan Mountains on polarimetric SAR images. Remote Sensing of Environment, 2014, 145, 47-54.	11.0	18
35	The measurement and model construction of complex permittivity of vegetation. Science China Earth Sciences, 2014, 57, 729-740.	5.2	19
36	Land Cover Classification of Quad-Polarimetric RADARSAT-2 SAR Image Based on Modified Subspace Method. Canadian Journal of Remote Sensing, 2014, 40, 271-277.	2.4	0

LIZHE

#	Article	IF	CITATIONS
37	A simplified physically-based algorithm for surface soil moisture retrieval using AMSR-E data. Frontiers of Earth Science, 2014, 8, 427-438.	2.1	16
38	Polarimetric analysis of multi-temporal RADARSAT-2 SAR images for wheat monitoring and mapping. International Journal of Remote Sensing, 2014, 35, 3840-3858.	2.9	25
39	Hemispheric-scale comparison of monthly passive microwave snow water equivalent products. Journal of Applied Remote Sensing, 2014, 8, 084688.	1.3	9
40	Orientation of Spaceborne SAR Stereo Pairs Employing the RPC Adjustment Model. IEEE Transactions on Geoscience and Remote Sensing, 2011, 49, 2782-2792.	6.3	29
41	Application of RPC model for InSAR phase evaluation. , 2011, , .		Ο
42	RPC-based adjustment model for COSMO-SkyMed stereo slant/ground-range images. , 2010, , .		2
43	Dynamic analysis of the Wenchuan Earthquake disaster and reconstruction with 3-year remote sensing data. International Journal of Digital Earth, 2010, 3, 355-364.	3.9	16